Radial and Axial Displacement of the Initially-Tensioned Orthotropic Arterial Wall Under the Influence of Harmonics and Wave Reflection

Zhili Hao
Department of Mechanical and Aerospace Engineering,
Old Dominion University,
Norfolk, VA 23529
e-mail: zlhao@odu.edu

This study examines radial and axial displacement of the arterial wall under the influence of harmonics and wave reflection for the role of axial wall displacement in pulsatile wave propagation. The arterial wall is modeled as an initially-tensioned thin-walled orthotropic tube. In conjunction with three pulsatile parameters in blood flow, a free wave propagation analysis is conducted on the governing equations of the arterial wall and no-slip conditions at the blood-wall interface to obtain the frequency equation and pulsatile parameter expressions under different harmonics. The influence of wave reflection is then added to pulsatile parameter expressions. With the harmonic values of measured pulsatile pressure and blood flow rate at the ascending aorta in the literature, the waveforms of radial wall displacement, axial wall displacement, and wall shear stress are calculated under different orthotropicity and axial initial tension. The developed theory and calculated results indicate that (1) difference in waveform between blood flow rate, wall shear stress, and axial wall displacement is caused by harmonics, rather than wave reflection; (2) Axial wall displacement does not affect blood flow rate, radial wall displacement, and wall shear stress; (3) Besides wall shear stress, radial wall displacement gradient also contributes to axial wall displacement and its contribution is adjusted by axial initial tension; (4) different wave reflections only noticeably affect the maximum and minimum values of wall shear stress; and (5) The amplitude and waveform of axial wall displacement are predominantly dictated by axial elasticity and axial initial tension, respectively. [DOI: 10.1115/1.4054883]

Keywords: arterial wall, orthotropicity, initial tension, radial displacement, axial displacement, wave reflection, harmonics, atherosclerosis

1 Introduction

Blood circulation in the cardiovascular (CV) system is essentially pulsatile wave propagation in arteries [1]. Clinical studies have identified the importance of radial displacement of the arterial wall in pulsatile wave propagation and established its clinical value for detection of atherosclerosis. Yet, radial-displacement-based clinical measures remain limited in early prediction of atherosclerosis [2–7]. In recent years, axial displacement of the arterial wall is found to be comparable in amplitude to radial displacement of the arterial wall [2–7], be a more sensitive measure of subclinical atherosclerosis, and correlate with CV risk factors differently, as compared with radial-displacement-based clinical measures [6]. Meanwhile, studies on excised arteries find that axial initial tension and axial stress of the arterial wall affect arterial wall remodeling and growth and vascular homeostasis [8,9], but their measurement on live subjects is not established. Additionally, circumferential initial tension (i.e., diastolic blood pressure) of the arterial wall is found to affect the wave propagation velocity [10]. Yet, in recent decades, the theories and related numerical models on arterial pulsatile wave propagation are focused on the governing equations of blood flow in an artery and include only radial displacement of the arterial wall as a boundary condition [1], and thus are unsuitable to examine axial displacement and axial initial tension of the arterial wall for their role in pulsatile wave propagation.

The problem with blood circulation in the CV system has a long history. With radial and axial displacement of the arterial wall being considered, the problem of pulsatile wave propagation in arteries was extensively examined by many researchers in the 1950–1960s [11–15]. By adopting a free wave propagation approach, Womersley [11] laid out the theoretical framework and derived the wave expressions for three pulsatile parameters in blood flow, with the arterial wall modeled as a thin-walled isotropic tube with no initial tension and blood flow treated as an incompressible, Newtonian fluid. Later on, many factors arising from the physiological reality in the CV system were added to this framework [12–15]. For instance, Atabek [12] modeled the arterial wall as a thin-walled orthotropic tube with two initial tensions, and Mirsky [13] modeled the arterial wall as a thick-walled orthotropic tube with no initial tension but considered the influence of harmonics and wave reflection. Regardless of the tube model used, the wave expressions for three pulsatile parameters in blood flow derived by Womersley remain the same [14]. However, these theoretical studies were never applied to clinical studies, since axial displacement of the arterial wall was considered to be negligible at that time, as compared with radial displacement of the arterial wall. The theories on arterial pulsatile wave propagation assume that the mechanical properties of the arterial wall do not vary along with its thickness [1,12,13]. This assumption is consistent with clinical studies, in which the arterial wall displacement is

Contributed by the Applied Mechanics Division Technical Committee on Dynamics & Control of Structures & Systems (AMD-DCSS) of ASME for publication in the Journal of Engineering and Science in Medical Diagnostics and Therapy. Manuscript received May 14, 2022; final manuscript received June 20, 2022; published online July 19, 2022. Editor: Ahmed Al-Jumaily.

measured at one point along the wall thickness to represent the collective behavior of the arterial wall at an artery site [1–7]. It should be noted that various constitutive models of the arterial wall are also developed that consider three layers and different biological components in the arterial wall along its thickness [16,17], but these models are aimed to examine the relation of mechanical function to biological function in the arterial wall and are unpractical for clinical studies yet.

In this study, the related theories from Atabek [12] and Mirsky [13] are combined and improved for revealing the role of axial displacement and two initial tensions of the arterial wall in pulsatile wave propagation under the influence of harmonics and wave reflection. The arterial wall is modeled as an initially-tensioned thin-walled orthotropic tube for examining the influence of harmonics on the wave velocity and pulsatile parameters with mathematical clarity. Afterward, the influence of wave reflection is added to pulsatile parameter expressions. With the harmonic values of measured pulsatile pressure and blood flow rate at the ascending aorta (AA) in the literature [13], the waveforms of radial wall displacement, axial wall displacement, and wall shear stress are calculated under different orthotropicity and axial initial tensions. The results are compared with Atabek and Mirky's studies, the author's previous associated study [18], as well as the related numerical studies [19,20]. The results are utilized to explain some related clinical findings and their physiological implications and possible clinical applications are further discussed.

2 Materials and Methods

2.1 Arterial Wall Basics and Assumptions. The arterial wall has a layered anatomical structure and is initially tensioned in the axial direction, due to its anatomy [9], and in the circumferential direction, due to diastolic blood pressure (DBP). As such, the arterial wall is modeled as an initially-tensioned thin-walled orthotropic tube. As shown in Fig. 1(*a*), the arterial wall geometry includes the inner radius a at DBP and thickness h [12]. The arterial wall has elasticity E_θ and initial tension per unit length $T_{\theta 0}$ in the circumferential direction, and elasticity E_x and initial tension per unit length T_{x0} in the axial direction (x-axis). During the time t of a pulse cycle, the arterial wall at a fixed axial-position x undergoes radial and axial motion, and thus has two pulsatile parameters: radial wall displacement $\eta(x,t)$ and axial wall displacement $\xi(x,t)$. The blood flow in the artery is assumed to be an incompressible Newtonian fluid and has three pulsatile parameters: radial blood flow velocity $w(r,x,t)$, axial blood flow velocity $u(r,x,t)$, and pulsatile blood pressure $\Delta p(r,x,t)$, where the radial coordinate r varies within $r \in (0, a)$.

Three fundamental assumptions for arterial pulsatile wave propagation are that: (1) The five pulsatile parameters are axisymmetric and small perturbations; (2) Change of the inner radius of the arterial wall is negligible during arterial wall motion so that the conditions and stresses at the blood-wall interface are calculated at $r = a$; and 3). The inner radius of the arterial wall is much smaller than the pulse wavelength λ ($a \ll \lambda$) and thus $\Delta p(r,x,t)$ is independent of r and becomes $\Delta p(x,t)$ [11–15].

2.2 Wave Expressions for Three Pulsatile Parameters in Blood Flow. The governing equations of blood flow in an artery include the continuity equation and the Navier–Stoke equations in the axial (x-axis) and radial (r-axis) directions [11]

$$\frac{\partial w}{\partial r} + \frac{w}{r} + \frac{\partial u}{\partial x} = 0 \tag{1a}$$

$$\rho_b \frac{\partial w}{\partial t} = -\frac{\partial \Delta p}{\partial r} + \mu\left(\frac{\partial^2 w}{\partial r^2} + \frac{1}{r}\frac{\partial w}{\partial r} - \frac{w}{r^2} + \frac{\partial^2 w}{\partial x^2}\right) \tag{1b}$$

$$\rho_b \frac{\partial u}{\partial t} = -\frac{\partial \Delta p}{\partial x} + \mu\left(\frac{\partial^2 u}{\partial r^2} + \frac{1}{r}\frac{\partial u}{\partial r} + \frac{\partial^2 u}{\partial x^2}\right) \tag{1c}$$

where ρ_b and μ denote the blood density and viscosity, respectively.

Womersley derived the solution to Eq. (1)—the wave expressions for w, u, and Δp [11]

$$w = \left[-\Delta p_0 \frac{\beta_0^2 r}{2\mu\alpha_0^2} + B\frac{\beta_0}{\alpha_0 J_0(\alpha_0)} J_1(\alpha_0 r/a)\right] \cdot e^{i(n\omega t - kx)} \tag{2a}$$

$$u = \left[-\Delta p_0 \frac{\beta_0 a}{\mu\alpha_0^2} + B\frac{J_0(\alpha_0 r/a)}{J_0(\alpha_0)}\right] \cdot e^{i(n\omega t - kx)} \tag{2b}$$

$$\Delta p = \Delta p_0 \cdot e^{i(n\omega t - kx)} \tag{2c}$$

where $\alpha_0^2 = i^3\alpha^2$ with $\alpha = a\sqrt{\rho_b n\omega/\mu}$ being Womersely number [11] and $\beta_0 = ian\omega/c = i\beta$ with n being the n-th harmonics of the heart rate; ω and $k = n\omega/c$ are the angular frequency of the heart rate and the nth wave number, respectively, where c is the wave velocity of the nth harmonic term of a pulse signal.

2.3 Problem Formulation for Radial and Axial Displacement of the Arterial Wall. In Atabek's work [12], the governing equations of the arterial wall for its radial and axial motion are given as

$$\rho h\frac{\partial^2 \eta}{\partial t^2} = \left\{\Delta p - 2\mu \cdot \frac{\partial w}{\partial r}\right\}_{r=a} + T_{\theta 0} \cdot \frac{\eta}{a^2} + T_{x0} \cdot \frac{\partial^2 \eta}{\partial x^2} - \frac{E_\theta h}{1 - \upsilon_\theta \upsilon_x} \cdot \left\{\frac{\eta}{a^2} + \frac{\upsilon_x}{a} \cdot \frac{\partial \xi}{\partial x}\right\} \tag{3a}$$

$$\rho h\frac{\partial^2 \xi}{\partial t^2} = -\mu\left\{\frac{\partial u}{\partial r} + \frac{\partial w}{\partial x}\right\}_{r=a} + \frac{\gamma E_\theta h}{1 - \upsilon_\theta \upsilon_x} \cdot \left\{\frac{\partial^2 \xi}{\partial x^2} + \frac{\upsilon_\theta}{a} \cdot \frac{\partial \eta}{\partial x}\right\} + \frac{T_{x0} - T_{\theta 0}}{a} \cdot \frac{\partial \eta}{\partial x} \tag{3b}$$

where ρ, υ_θ, and υ_x denote the density, circumferential Poisson's ratio, and axial Poisson's ratio of the arterial wall, respectively; and $\gamma = E_x/E_\theta$. The first term on the right side of Eq. (3*b*) is wall shear stress (wss) τ_w.

The value of Possion's ratio of the arterial wall in vivo is unknown [21] and is ignored for obtaining the value of E_θ in clinical studies [1–7]. The great similarity in the measured waveforms of $\Delta p(t)$ and $\eta(t)$ at an artery (a fixed x-position) [1] might indicate

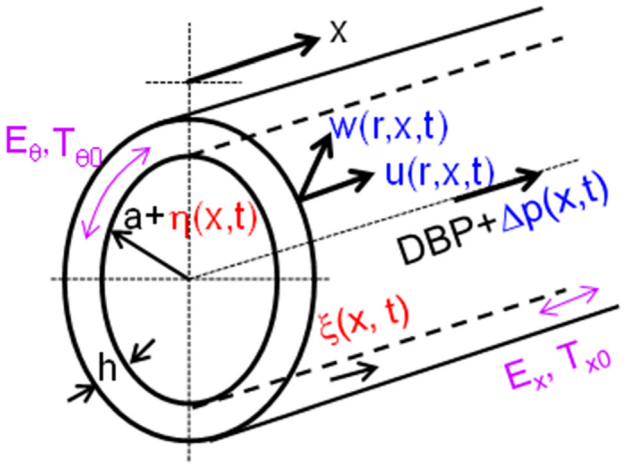

Fig. 1 Schematics of an artery: arterial wall geometries: inner radius *a* at DBP and thickness *h*; arterial wall mechanical properties: E_x, T_{x0}, E_θ, and $T_{\theta 0}$; three pulsatile parameters in blood flow: $w(r,x,t)$, $u(r,x,t)$, and $\Delta p(x,t)$; and two pulsatile parameters in the arterial wall: $\eta(x,t)$ and $\xi(x,t)$

that the contribution of $v_x \cdot \partial\xi/\partial x$ to $\eta(x,t)$ is negligible in Eq. (3*a*). Thus, it is reasonable to assume $v_x = 0$. As compared with the rest terms, the inertial term, the T_{x0}-associated term, and the term associated with radial blood flow velocity are small quantities in Eq. (3*a*). Then, Eq. (3*a*) is reduced to

$$0 = \Delta p - (E_\theta h - T_{\theta 0}) \cdot \frac{\eta}{a^2} \tag{4a}$$

According to Eq. (3*b*), there are three sources for causing $\xi(x,t)$: τ_w and two $\partial\eta/\partial x$ terms: one associated with v_θ, and the other associated with $(T_{x0}-T_{\theta 0})$. By adjusting the value of T_{x0}, the contribution of the $\partial\eta/\partial x$ term associated with v_θ to $\xi(x,t)$ can be included in the contribution of the $\partial\eta/\partial x$ term associated with $(T_{x0}-T_{\theta 0})$ to $\xi(x,t)$, without altering the waveform of $\xi(t)$. Therefore, it is also assumed that $v_\theta = 0$ and Eq. (3*b*) is reduced to [18]

$$\rho h \frac{\partial^2 \xi}{\partial t^2} = \gamma E_\theta h \cdot \frac{\partial^2 \xi}{\partial x^2} - \tau_w + \frac{T_{x0} - T_{\theta 0}}{a} \cdot \frac{\partial \eta}{\partial x} \quad \text{with}$$
$$\tau_w = \mu \left\{ \frac{\partial u}{\partial r} + \frac{\partial w}{\partial x} \right\}_{r=a} \tag{4b}$$

No-slip conditions at the blood-wall interface demand the blood flow velocities to be equal to the arterial wall velocities in the radial and axial directions at the blood-wall interface [11–13]

$$w_{r=a} = \frac{\partial \eta}{\partial t} \tag{4c}$$

$$u_{r=a} = \frac{\partial \xi}{\partial t} \tag{4d}$$

2.4 A Free Wave Propagation Analysis for Wave Velocity and Pulsatile Parameters. The wave expressions for $\eta(x,t)$ and $\xi(x,t)$ are

$$\eta = \eta_0 \cdot e^{i(n\omega t - kx)} \tag{5a}$$

$$\xi = \xi_0 \cdot e^{i(n\omega t - kx)} \tag{5b}$$

Four constant unknowns: Δp_0, B, η_0, and ξ_0, are involved in the wave expressions for the five pulsatile parameters in Eqs. (2) and (5). Substituting these wave expressions into Eq. (4) leads to a 4×4 matrix equation with a vector of the four constant unknowns

$$\begin{bmatrix} -\frac{\beta_0 a}{\mu \alpha_0^2} & 1 & 0 & -in\omega \\ -\frac{\beta_0^2 a}{2\mu\alpha_0^2} & \frac{1}{2}\beta_0 F_{10} & -in\omega & 0 \\ 1 & 0 & (\tau_{\theta 0} - 1)\frac{E_\theta h}{a^2} & 0 \\ -\frac{\beta_0^3}{2\alpha_0^2} & \frac{\mu\alpha_0^2}{2a} F_{10} & -(\tau_{x0} - \tau_{\theta 0}) E_\theta h \frac{\beta_0}{a^2} & \frac{\gamma E_\theta h}{1 - v_\theta v_x}\frac{\beta_0^2}{a^2} + \rho h (n\omega)^2 \end{bmatrix} \begin{Bmatrix} \Delta p_0 \\ B \\ \eta_0 \\ \xi_0 \end{Bmatrix} = \begin{Bmatrix} 0 \\ 0 \\ 0 \\ 0 \end{Bmatrix} \tag{6}$$

where

$$\tau_{\theta 0} = T_{\theta 0}/(E_\theta h), \quad \tau_{x0} = T_{x0}/(E_\theta h), \quad F_{10} = \frac{2J_1(\alpha_0)}{\alpha_0 J_0(\alpha_0)} \tag{7}$$

Note that τ_{x0} and $\tau_{\theta 0}$ are normalized initial tensions, and F_{10} is due to fluid-loading and takes complex values.

A nonzero solution for the four constant unknowns demands that the determinant of the 4×4 matrix in Eq. (6) be equal to zero, leading to the frequency equation

$$\{F_{10}(2\tau_{x0} - \tau_{\theta 0} - 1) - (1 - F_{10})(1 - \tau_{\theta 0})K - 4\gamma\}\frac{c_0^2}{c^2} + 4(1 - F_{10}) \cdot \{(1 - \tau_{\theta 0})\gamma\}\frac{c_0^4}{c^4} + F_{10} + 2K = 0 \tag{8}$$

where

$$c_0 = \sqrt{\frac{E_\theta h}{2\rho_b a}}, \quad K = \frac{\rho h}{\rho_b a} \tag{9}$$

The two roots of Eq. (8) correspond to the Young wave (c_1) and the Lamb wave (c_2). The wave velocity (or phase velocity) of the Young wave and the Lamb wave becomes *real*(c_1) and *real*(c_2), respectively. The wave transmission per wavelength is then calculated as $exp(-2\pi Y/X)$, with $c = X + Yi$ (X and Y take real values). The influence of harmonics on the wave velocity arises from F_{10}.

Removal of F_{10}, τ_{x0}, and $\tau_{\theta 0}$ in Eq. (8) separates the Young wave and the Lamb wave and leads to the wave velocity of uncoupled radial displacement and axial displacement of the arterial wall, respectively

$$c_1 = c_0 = \sqrt{\frac{E_\theta h}{2\rho_b a}} = PWV \text{ (uncoupled Young wave)} \tag{10a}$$

$$c_2 = \sqrt{\frac{E_x}{\rho}} = c_L \text{ (uncoupled Lamb wave)} \tag{10b}$$

Note that c_1 is reduced to the Moens–Korteweg formula for pulse wave velocity (PWV), which is commonly used in clinical studies [1–7], and c_2 is reduced to longitudinal elastic wave velocity c_L [15].

By assuming $\xi(x,t) = 0$ and then $u_{r=a} = 0$, Eq. (6) predicts only the Young wave with its wave velocity [18]

$$c_1 = c_0 \sqrt{(1 - F_{10})(1 - \tau_{\theta 0})} \tag{11}$$

Comparison of Eqs. (10*a*) and (11) implies that circumferential initial tension (or DBP) lowers the Young wave velocity and fluid-loading causes wave attenuation.

While the Young wave is excited by pulsatile pressure, the Lamb wave is excited by the axial stress in the arterial wall [15]. In clinical studies, all the measured pulsatile parameters are

considered in the Young wave. Although experimental studies on excised arteries validated the existence of the Lamb wave [22], the Lamb wave measurement has not been established in clinical studies. As such, only the Young wave is analyzed in this study. Unless otherwise stated, all the parameters discussed in the rest of this section are for the Young wave. With Δp_0 as the known, the rest three constant unknowns can be derived from Eq. (6)

$$\eta_0 = \frac{a}{2c^2\rho_b}(1+mF_{10})\Delta p_0 \quad \xi_0 = \frac{(1+m)}{in\omega c\rho_b}\Delta p_0 \quad B = \frac{m}{c\rho_b}\Delta p_0 \tag{12}$$

where

$$m = \frac{\frac{c^2}{c_0^2} + (\tau_{\theta 0} - 1)}{(1-\tau_{\theta 0})F_{10}} \tag{13}$$

The ratio of η_0/ξ_0 represents the mode shape of the arterial wall in the Young wave

$$\frac{\eta_0}{\xi_0} = \frac{in\omega a(1+mF_{10})}{2c(1+m)} \tag{14}$$

2.5 Pulsatile Parameters With and Without Wave Reflection. With no wave reflection, only a forward pulsatile pressure wave exists in an artery

$$\Delta p(x,t) = Ae^{i(nwt-kx)} \tag{15a}$$

Consequently, blood flow rate $Q(x,t)$, radial wall displacement $\eta(x,t)$, and axial wall displacement $\xi(x,t)$, and wall shear stress $\tau_w(x,t)$ are

$$Q(x,t) = \int_0^a u2\pi r dr = \frac{1+mF_{10}}{c\rho_b}\pi a^2 \cdot Ae^{i(nwt-kx)} \tag{15b}$$

$$\eta(x,t) = \frac{(1+mF_{10})a}{2c^2\rho_b} \cdot Ae^{i(nwt-kx)} \tag{15c}$$

$$\xi(x,t) = \frac{(1+m)}{in\omega c\rho_b} \cdot Ae^{i(nwt-kx)} \tag{15d}$$

$$\tau_w(x,t) = \frac{in\omega amF_{10}}{2c} \cdot Ae^{i(nwt-kx)} \tag{15e}$$

With wave reflection, the pulsatile pressure in an artery becomes [1,13]

$$\Delta p(x,t) = Ae^{i(n\omega t-kx)} + A'e^{i(n\omega t+kx)} \tag{16a}$$

where $Ae^{i(n\omega t-kx)}$ and $A'e^{i(n\omega t+kx)}$ represent the forward wave and the backward wave of $\Delta p(x,t)$, respectively. Based on Eqs. (1) and (4), blood flow rate, radial wall displacement, axial wall displacement, and wall shear stress become

$$Q(x,t) = \left\{\frac{1}{c\rho_b}(1+mF_{10})\right\}\pi a^2\left(Ae^{i(n\omega t-kx)} - A'e^{i(n\omega t+kx)}\right) \tag{16b}$$

$$\eta(x,t) = \frac{a}{2c^2\rho_b}(1+mF_{10})\left(Ae^{i(n\omega t-kx)} + A'e^{i(n\omega t+kx)}\right) \tag{16c}$$

$$\xi(x,t) = \frac{(1+m)}{in\omega c\rho_b}\left(Ae^{i(n\omega t-kx)} - A'e^{i(n\omega t+kx)}\right) \tag{16d}$$

$$\tau_w(x,t) = \frac{in\omega amF_{10}}{2c}\left(Ae^{i(n\omega t-kx)} - A'e^{i(n\omega t+kx)}\right) \tag{16e}$$

Wave reflection augments $\Delta p(x,t)$ and $\eta(x,t)$, due to their radial direction, but reduces $Q(x,t)$, $\xi(x,t)$, and $\tau_w(x,t)$, due to their axial direction. Note that the amplitudes of axial wall displacement and wall shear stress reveal different explicit dependence on harmonics (or n). In contrast, the amplitudes of blood flow rate and radial wall displacement do not show explicit dependence on harmonics (or n).

Two direct clinical measures at an artery (fixed x-position) are $\Delta p(t)$ and $Q(t)$. Based on Eqs. (16*a*) and (16*b*), the forward and backward waves of $\Delta p(t)$ can be derived from the measured $\Delta p(t)$ and $Q(t)$

$$Ae^{i(n\omega t-kx)} = \frac{\Delta p(t)}{2} + Z_c\frac{Q(t)}{2\pi a^2} \tag{17a}$$

$$A'e^{i(n\omega t+kx)} = \frac{\Delta p(t)}{2} - Z_c\frac{Q(t)}{2\pi a^2} \tag{17b}$$

where Z_c is the characteristic impedance defined as Ref. [23]

$$Z_c = \frac{\Delta p}{Q}\pi a^2 = \frac{c\rho_b}{(1+mF_{10})} \tag{18}$$

3 Calculated Results

Although $\xi(t)$ is measured at the carotid artery (CA) [2–7], the harmonic values of measured pulsatile pressure and blood flow rate waveforms are only available at the ascending aorta (AA) in the literature [13]. As such, we calculate the wave velocity and above-derived pulsatile parameters at the AA. The values for the AA are $E_\theta = 400$ kPa, $a = 13$ mm, and $h = 2$ mm, and the fundamental frequency of the heart rate is 1.25 Hz (or 75 beats per minute) [13,24]. Circumferential initial tension $T_{\theta 0}$ = DBP×a is assumed at $\tau_{\theta 0} = 0.1$. The values of T_{x0} and E_x in vivo are unknown. Based on Eq. (4*b*), $\tau_{x0} = 0.1$ is utilized to examine the situation where only τ_w causes $\xi(t)$, and $\tau_{x0} = 0.2$ is utilized to examine the situation where both τ_w and the $\partial\eta/\partial x$ term with a factor of $(T_{x0}-T_{\theta 0})$ cause $\xi(t)$. The value of $\gamma = E_x/E_\theta$ is varied to examine how orthotropicity affects the pulsatile parameters. Unless otherwise specified, the calculated pulsatile parameters are for the Young wave.

3.1 Influence of Harmonics on Wave Velocity and Pulsatile Parameters With No Wave Reflection. As shown in Table 1, wave velocity in the Young wave and the Lamb wave does not vary with harmonics, and the wave transmission in the two waves increases with the higher harmonics. The wave velocity and wave transmission in the Young wave are not affected by the values of E_x and τ_{x0}. The wave velocity and wave transmission in the Young wave with $\xi(x,t) = 0$ are also calculated and summarized in Table 2, showing that the inclusion of axial wall displacement does not affect the wave velocity and transmission in the Young wave.

As shown in Table 3, $\xi(x,t)$ is not negligible in the Young wave, and the ratio of η_0/ξ_0 increases dramatically with the higher harmonics. This ratio increases with E_x and also varies with τ_{x0}. As shown in Table 4, the ratio of η_0/ξ_0 in the Lamb wave also varies with harmonics, but this ratio is about $\sim 10^{-3}$, indicating that $\eta(x,t)$ can be considered to be solely from the Young wave. Based on the calculated values and phases of $(1+mF_{10})$ in the expressions for $Q(x,t)$ and $\eta(x,t)$ in Eqs. (15*b*) and (15*c*) in Table 5, $Q(x,t)$ and $\eta(x,t)$ are overall harmonics-independent, in the sense that they follow the same harmonic distribution of the pulsatile pressure. Without wave reflection, the phase shifts of $Q(x,t)$ and $\eta(x,t)$ relative to $\Delta p(x,t)$ are negligible. As shown in Table 6(*a*),

Table 1 Wave velocity and wave transmission in the Young wave and the Lamb wave at the AA under

(a) $\gamma = 1/3$

	$\tau_{\theta 0} = 0.1$, $\tau_{x0} = 0.1$				$\tau_{\theta 0} = 0.1$, $\tau_{x0} = 0.2$			
n	Real(c_1) (m/s)	Exp ($-2\pi Y_1/X_1$)	Real (c_2) (m/s)	Exp($-2\pi Y_2/X_2$)	Real(c_1) (m/s)	Exp($-2\pi Y_1/X_1$)	Real (c_2) (m/s)	Exp ($-2\pi Y_2/X_2$)
1	4.93	0.76	9.94	0.57	4.97	0.79	9.87	0.54
2	4.99	0.83	10.30	0.65	5.01	0.86	10.24	0.63
3	5.01	0.86	10.46	0.69	5.03	0.88	10.42	0.67
4	5.03	0.88	10.56	0.72	5.05	0.90	10.52	0.70
5	5.04	0.89	10.63	0.74	5.06	0.91	10.60	0.73
6	5.05	0.90	10.69	0.76	5.06	0.92	10.65	0.74
7	5.05	0.91	10.73	0.77	5.07	0.93	10.70	0.76
8	5.06	0.92	10.76	0.78	5.08	0.93	10.73	0.77
9	5.06	0.92	10.79	0.79	5.08	0.93	10.76	0.78
10	5.07	0.92	10.81	0.80	5.09	0.94	10.78	0.79

(b) $\gamma = 1$

	$\tau_{\theta 0} = 0.1$, $\tau_{x0} = 0.1$				$\tau_{\theta 0} = 0.1$, $\tau_{x0} = 0.2$			
n	Real(c_1) (m/s)	Exp ($-2\pi Y_1/X_1$)	Real (c_2) (m/s)	Exp($-2\pi Y_2/X_2$)	Real(c_1) (m/s)	Exp($-2\pi Y_1/X_1$)	Real (c_2) (m/s)	Exp ($-2\pi Y_2/X_2$)
1	4.93	0.77	17.22	0.56	4.94	0.78	17.18	0.55
2	4.99	0.84	17.84	0.64	4.99	0.85	17.81	0.63
3	5.01	0.87	18.12	0.69	5.02	0.87	18.10	0.68
4	5.03	0.88	18.30	0.72	5.03	0.89	18.28	0.71
5	5.04	0.90	18.42	0.74	5.05	0.90	18.40	0.73
6	5.05	0.91	18.51	0.76	5.05	0.91	18.49	0.75
7	5.05	0.91	18.58	0.77	5.06	0.92	18.56	0.77
8	5.06	0.92	18.63	0.78	5.07	0.92	18.62	0.78
9	5.06	0.92	18.68	0.79	5.07	0.93	18.67	0.79
10	5.07	0.93	18.72	0.80	5.08	0.93	18.71	0.80

(c) $\gamma = 3$

	$\tau_{\theta 0} = 0.1$, $\tau_{x0} = 0.1$				$\tau_{\theta 0} = 0.1$, $\tau_{x0} = 0.2$			
n	Real(c_1) (m/s)	Exp ($-2\pi Y_1/X_1$)	Real (c_2) (m/s)	Exp($-2\pi Y_2/X_2$)	Real(c_1) (m/s)	Exp($-2\pi Y_1/X_1$)	Real (c_2) (m/s)	Exp ($-2\pi Y_2/X_2$)
1	4.93	0.78	29.82	0.56	4.93	0.78	29.80	0.55
2	4.99	0.84	30.89	0.64	4.99	0.84	30.88	0.64
3	5.01	0.87	31.39	0.68	5.01	0.87	31.38	0.68
4	5.03	0.89	31.69	0.71	5.03	0.89	31.68	0.71
5	5.04	0.90	31.90	0.74	5.04	0.90	31.89	0.74
6	5.05	0.91	32.06	0.76	5.05	0.91	32.05	0.75
7	5.05	0.91	32.18	0.77	5.06	0.91	32.17	0.77
8	5.06	0.92	32.28	0.78	5.07	0.92	32.27	0.78
9	5.06	0.92	32.36	0.79	5.07	0.92	32.35	0.79
10	5.07	0.93	32.43	0.80	5.08	0.93	32.42	0.80

the characteristic impedance does not vary with harmonics and can be treated as a real value. Since the characteristic impedance is a quantitative measure of wave reflection, Table 6(*a*) indicates that γ and τ_{x0} have no influence on wave reflection.

3.2 Calculated Waveforms of Pulsatile Parameters With Harmonics and Wave Reflection. The $\Delta p(t)$ and $Q(t)$ waveforms at an artery can be approximated by their first ten harmonics of the heart rate [13]

$$\Delta p(t) = \sum_{n=1}^{10} \Delta p_n \sin(n\omega t + \theta_n) \tag{19a}$$

$$\Delta Q(t) = \sum_{n=1}^{10} Q_n \sin(n\omega t + \theta_n) \tag{19b}$$

Table 7 summarizes the harmonic values for the measured $\Delta p(t)$ and $Q(t)$ waveforms at the AA in the literature [13]. The

Table 2 Wave velocity and wave transmission in the Young wave at the AA with $\xi(x, t) = 0$

n	1	2	3	4	5	6	7	8	9	10
Real (c_1) (m/s)	4.93	4.99	5.01	5.03	5.04	5.05	5.05	5.06	5.06	5.07
Exp($-2\pi Y_1/X_1$)	0.78	0.84	0.87	0.89	0.90	0.91	0.91	0.92	0.92	0.93

Table 3 Ratio of η_0/ξ_0 in the Young wave at the AA

	$\gamma = 1/3$		$\gamma = 1$		$\gamma = 3$	
n	$\tau_{\theta 0} = 0.1, \tau_{x0} = 0.1$	$\tau_{\theta 0} = 0.1, \tau_{x0} = 0.2$	$\tau_{\theta 0} = 0.1, \tau_{x0} = 0.1$	$\tau_{\theta 0} = 0.1, \tau_{x0} = 0.2$	$\tau_{\theta 0} = 0.1, \tau_{x0} = 0.1$	$\tau_{\theta 0} = 0.1, \tau_{x0} = 0.2$
1	0.11	0.07	0.40	0.26	1.28	0.82
2	0.31	0.13	1.13	0.47	3.56	1.50
3	0.57	0.19	2.05	0.68	6.50	2.16
4	0.88	0.25	3.15	0.89	9.97	2.80
5	1.23	0.30	4.39	1.09	13.89	3.44
6	1.61	0.36	5.77	1.29	18.22	4.07
7	2.03	0.41	7.25	1.49	22.92	4.70
8	2.48	0.47	8.85	1.68	27.96	5.32
9	2.96	0.53	10.55	1.88	33.31	5.94
10	3.47	0.58	12.34	2.07	38.97	6.55

Table 4 Ratio of η_0/ξ_0 in the Lamb wave at the AA

	$\gamma = 1/3$		$\gamma = 1$		$\gamma = 3$	
n	$\tau_{\theta 0} = 0.1, \tau_{x0} = 0.1$	$\tau_{\theta 0} = 0.1, \tau_{x0} = 0.2$	$\tau_{\theta 0} = 0.1, \tau_{x0} = 0.1$	$\tau_{\theta 0} = 0.1, \tau_{x0} = 0.2$	$\tau_{\theta 0} = 0.1, \tau_{x0} = 0.1$	$\tau_{\theta 0} = 0.1, \tau_{x0} = 0.2$
1	7.08×10^{-4}	7.16×10^{-4}	3.37×10^{-4}	3.38×10^{-4}	1.84×10^{-4}	1.84×10^{-4}
2	9.61×10^{-4}	9.69×10^{-4}	4.62×10^{-4}	4.62×10^{-4}	2.52×10^{-4}	2.53×10^{-4}
3	1.16×10^{-3}	1.16×10^{-3}	5.57×10^{-4}	5.58×10^{-4}	3.05×10^{-4}	3.05×10^{-4}
4	1.32×10^{-3}	1.33×10^{-3}	6.38×10^{-4}	6.39×10^{-4}	3.49×10^{-4}	3.50×10^{-4}
5	1.46×10^{-3}	1.47×10^{-3}	7.09×10^{-4}	7.10×10^{-4}	3.88×10^{-4}	3.89×10^{-4}
6	1.59×10^{-3}	1.60×10^{-3}	7.73×10^{-4}	7.74×10^{-4}	4.24×10^{-4}	4.24×10^{-4}
7	1.71×10^{-3}	1.72×10^{-3}	8.32×10^{-4}	8.33×10^{-4}	4.56×10^{-4}	4.56×10^{-4}
8	1.83×10^{-3}	1.83×10^{-3}	8.87×10^{-4}	8.88×10^{-4}	4.87×10^{-4}	4.87×10^{-4}
9	1.93×10^{-3}	1.94×10^{-3}	9.39×10^{-4}	9.39×10^{-4}	5.15×10^{-4}	5.15×10^{-4}
10	2.03×10^{-3}	2.04×10^{-3}	9.88×10^{-4}	9.88×10^{-4}	5.42×10^{-4}	5.42×10^{-4}

characteristic impedance can also be approximated by the following expression [23]

$$\max\left(\frac{\partial \Delta p}{\partial t}\right) / \max\left(\frac{\partial Q}{\partial t}\right) \cdot \pi a^2 \tag{20}$$

The characteristic impedance based on Eq. (20) can be calculated without knowing the mechanical properties of the arterial wall and can be treated as the measured wave reflection, as opposed to its theoretical counterpart in Eq. (18). As shown in Table 6(*b*), the calculated values based on Eq. (20) reveal random variation with harmonics. The calculated values based on Eqs. (18) and (20) are relatively close to each other for the rest harmonics, except for the 2nd and 3rd harmonics. This may indicate that the mechanical properties of the arterial wall are embedded in the relation of measured $\Delta p(t)$ and $Q(t)$. Based on Eqs. (17) and Table 6, the forward and backward waves of $\Delta p(t)$ are calculated and consequently the forward and backward waves of $Q(t)$ are also obtained, as shown in Fig. 2. The difference in waveform between $\Delta p(t)$ and $Q(t)$ is solely due to wave reflection, irrelevant to the harmonics. Evidently, different wave reflections from Eqs. (18) and (20) lead to different forward and backward waves of $\Delta p(t)$ and $Q(t)$, but the sum of the two pulsatile parameters remains the same for different wave reflections, because of Eq. (17).

Together with their forward and backward waves, the calculated $\eta(t)$, $\xi(t)$, and $\tau_w(t)$ waveforms under isotropic conditions ($\gamma = 1$) are plotted in Figs. 3 and 4, with $\tau_{x0} = 0.1$ and $\tau_{x0} = 0.2$, respectively. The $\eta(t)$ waveform is the same as the $\Delta p(t)$ waveform, due to the same influence of wave reflection and harmonics-independence. While $\xi(t)$ is solely caused by $\tau_w(t)$ in Fig. 3, $\tau_w(t)$ and the $\partial\eta/\partial x$ term with a factor of $(T_{x0}\text{-}T_{\theta 0})$ both contribute to $\xi(t)$ in Fig. 4. Note that the $\eta(t)$ and $\tau_w(t)$ waveforms remain the same, regardless of the value of τ_{x0}. Yet, the $\xi(t)$ waveform is completely altered by the $\partial\eta/\partial x$ term with a factor of $(T_{x0}\text{-}T_{\theta 0})$,

Table 5 Calculated values and phases of $(1+mF_{10})$ at the AA

	$\gamma = 1/3$				$\gamma = 1$				$\gamma = 3$			
	$\tau_{\theta 0} = 0.1, \tau_{x0} = 0.1$		$\tau_{\theta 0} = 0.1, \tau_{x0} = 0.2$		$\tau_{\theta 0} = 0.1, \tau_{x0} = 0.1$		$\tau_{\theta 0} = 0.1, \tau_{x0} = 0.2$		$\tau_{\theta 0} = 0.1, \tau_{x0} = 0.1$		$\tau_{\theta 0} = 0.1, \tau_{x0} = 0.2$	
n	Value	Phase (°)	Value	Phase (°)	Value	Phase (°)	Value	Phase (°)	Value	Phase (°)	Value	Phase (°)
1	0.93	5.1	0.94	4.2	0.93	4.7	0.93	4.4	0.93	4.5	0.93	4.5
2	0.95	3.4	0.96	2.8	0.95	3.2	0.95	3.1	0.95	3.2	0.95	3.1
3	0.96	2.7	0.97	2.3	0.96	2.6	0.96	2.5	0.96	2.6	0.96	2.5
4	0.96	2.3	0.97	1.9	0.96	2.2	0.96	2.1	0.96	2.2	0.96	2.2
5	0.97	2.1	0.97	1.7	0.97	2.0	0.97	1.9	0.97	2.0	0.97	1.9
6	0.97	1.9	0.98	1.5	0.97	1.8	0.97	1.7	0.97	1.8	0.97	1.8
7	0.97	1.7	0.98	1.4	0.97	1.7	0.97	1.6	0.97	1.7	0.97	1.6
8	0.97	1.6	0.98	1.3	0.97	1.6	0.98	1.5	0.97	1.6	0.97	1.5
9	0.98	1.5	0.98	1.2	0.98	1.5	0.98	1.4	0.98	1.5	0.98	1.4
10	0.98	1.4	0.98	1.2	0.98	1.4	0.98	1.3	0.98	1.4	0.98	1.4

Table 6 Calculated results of the characteristic impedance Z_c at the AA

(a) Calculated values (unit: *Pa·s/m*) and phases based on Eq. (18)

	$\gamma = 1/3$				$\gamma = 1$				$\gamma = 3$			
	$\tau_{\theta 0} = 0.1, \tau_{x0} = 0.1$		$\tau_{\theta 0} = 0.1, \tau_{x0} = 0.2$		$\tau_{\theta 0} = 0.1, \tau_{x0} = 0.2$		$\tau_{\theta 0} = 0.1, \tau_{x0} = 0.2$		$\tau_{\theta 0} = 0.1, \tau_{x0} = 0.1$		$\tau_{\theta 0} = 0.1, \tau_{x0} = 0.2$	
n	Value	phase (°)	value	phase (°)	Value	phase (°)	Value	phase (°)	Value	phase (°)	value	phase (°)
1	5614	−2.5	5573	−2.1	5613	−2.3	5602	−2.2	5613	−2.3	5610	−2.2
2	5552	−1.7	5524	−1.4	5552	−1.6	5544	−1.5	5552	−1.6	5550	−1.6
3	5525	−1.4	5503	−1.1	5525	−1.3	5519	−1.2	5525	−1.3	5524	−1.3
4	5509	−1.2	5491	−1.0	5509	−1.1	5505	−1.1	5509	−1.1	5509	−1.1
5	5498	−1.0	5484	−0.9	5498	−1.0	5496	−1.0	5498	−1.0	5500	−1.0
6	5491	−0.9	5479	−0.8	5491	−0.9	5491	−0.9	5491	−0.9	5494	−0.9
7	5485	−0.9	5476	−0.7	5485	−0.8	5487	−0.8	5485	−0.8	5490	−0.8
8	5480	−0.8	5474	−0.7	5480	−0.8	5484	−0.7	5480	−0.8	5487	−0.8
9	5477	−0.8	5474	−0.6	5477	−0.7	5483	−0.7	5477	−0.7	5486	−0.7
10	5474	−0.7	5474	−0.6	5474	−0.7	5483	−0.7	5474	−0.7	5485	−0.7

(b) Calculated values (unit: Pa·s/m) based on Eq. (20)

n	1	2	3	4	5	6	7	8	9	10
Value	6070	2897	2775	5201	4346	4284	5203	6962	5199	3916

due to that the value of $1+m$ depends on harmonics under $\tau_{x0} = 0.1$, but remains unchanged with harmonics under $\tau_{x0} = 0.2$. Although the influence of wave reflection on $\tau_w(t)$ and $\xi(t)$ and $Q(t)$ is the same, the different harmonics-dependence of $\tau_w(t)$ and $\xi(t)$ and the harmonics-independence of $Q(t)$ makes the three waveforms different. Different wave reflections have no effect on the $\eta(t)$ waveform, but slightly affect the $\xi(t)$ waveform. The wave reflection based on Eq. (20) (small wave reflection) noticeably reduces the maximum and minimum values of $\tau_w(t)$, as compared with the wave reflection based on Eq. (18) (large wave reflection).

The influence of orthotropicity of the arterial wall on the $\eta(t)$, $\xi(t)$, and $\tau_w(t)$ waveforms is examined in Figs. 5 and 6, under $\tau_{x0} = 0.1$ and $\tau_{x0} = 0.2$, respectively. The $\eta(t)$ waveform with no axial wall displacement is also plotted in Figs. 5(*a*) and 6(*a*) for comparison. The $\eta(t)$ waveform at different values of γ and τ_{x0} and different wave reflections is exactly the same as the one with no axial wall displacement. Note that the wave reflection based on Eq. (18) is utilized for the $\tau_w(t)$ waveforms in Figs. 5(*c*) and 6(*c*), and the wave reflection based on Eq. (20) is used for the $\tau_w(t)$ waveforms in Figs. 5(*d*) and 6(*d*). The values of τ_{x0} and γ have negligible effect on the $\tau_w(t)$ waveform and amplitude. In contrast, the wave reflection based on Eq. (20) noticeably reduces the maximum and minimum values of $\tau_w(t)$ at different values of τ_{x0} and γ, as compared with the wave reflection based on Eq. (18). The value of γ has no effect on the $\xi(t)$ waveform but greatly affects the $\xi(t)$ amplitude at different values of τ_{x0}. Similarly, the $\xi(t)$ waveform is dictated by the value of τ_{x0} at different values of γ. Different wave reflections slightly adjust the $\xi(t)$ waveform at different γ values.

Table 7 The harmonic values of the measured pulsatile pressure and the blood flow rate at the AA in the literature (adapted from Ref. [13])

N		1	2	3	4	5	6	7	8	9	10
$\Delta p(t)$	Amplitude (Pa)	1372	480.2	235.2	78.4	147	137.2	49	78.4	78.4	29.4
	Phase (°)	311	258	212	212	197	96	325	140	5	214
$Q(t)$	Amplitude (cm^3/s)	120	88	45	8	18	17	5	6	8	4
	Phase (°)	9	289	208	161	185	99	347	109	356	223

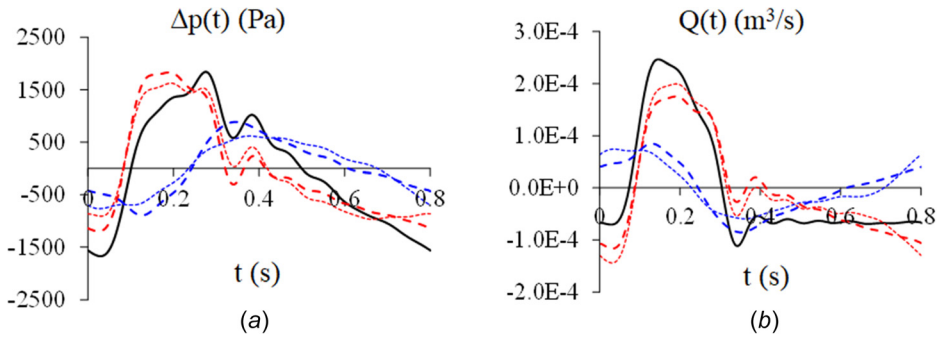

Fig. 2 Measured waveforms of: (*a*) pulsatile pressure $\Delta p(t)$ and (*b*) blood flow rate $Q(t)$ at the AA under $\gamma = 1$ and $\tau_{\theta 0} = \tau_{x0} = 0.1$ with the calculated forward waves and backward waves (dotted lines for the forward and backward waves: based on Eq. (20), dashed lines for the forward and backward waves: based on Eq. (18); solid line: sum of the forward and back waves)

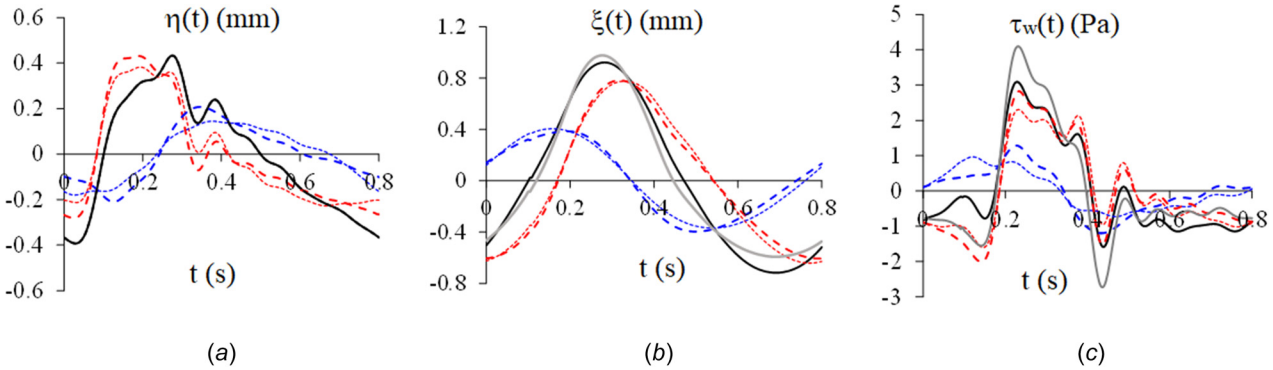

Fig. 3 Calculated waveforms of: (*a*) radial wall displacement $\eta(t)$ and (*b*) axial wall displacement $\xi(t)$ and (*c*) wall shear stress $\tau_w(t)$ at the AA under $\gamma = 1$ and $\tau_{\theta 0} = \tau_{x0} = 0.1$ with the forward and backward waves (dotted lines for the forward and backward waves: based on Eq. (20), dashed lines for the forward and backward waves: based on Eq. (18); solid black line: sum of the forward and backward waves based on Eq. (20), solid gray line: sum of the forward and backward waves based on Eq. (18))

4 Discussion

4.1 Comparison With the Relevant Studies in the Literature. In Atabek's study [12], the ratio of η_0/ξ_0 was examined only at the fundamental frequency of the heart rate. Upon finding that ξ_0 was unpractially large, as compared with η_0, neighboring tissue at the outer side of the arterial wall was then added to Eq. (4(*b*)) as three mechanical constraints (inertial, elastic, and damping) to lower ξ_0. Yet, the addition of the mechanical constraints alters longitudinal elastic wave propagation as the nature of axial wall displacement. Moreover, addition of these constraints is inconsistent with the governing equation of radial wall displacement, where circumferential elasticity has factored in the constraints of neighboring tissue in the radial direction. Atabek's study examined wave velocity and transmission and the ratio of η_0/ξ_0, but did not examine blood flow rate and wall shear stress, and the influence of harmonics and wave reflection on these pulsatile parameters.

In Mirsky's study [13], the arterial wall was modeled as a thick-walled tube with no initial tension and the influence of harmonics and wave reflection on pulsatile parameters was considered. With the harmonic values for $\Delta p(t)$ and $Q(t)$ at the AA in Table 7, $\eta(t)$ was found to be irrelevant to axial wall displacement under isotropic and orthotropic conditions, but $\tau_w(t)$ was not examined in that study. The $\xi(t)$ waveform in Fig. 5 is a little bit similar to the $\xi(t)$ waveform with Poisson's ratio being zero in Mirsky's study, and the difference between the two might be due to the difference in the tube models used. Due to a lack of mathematical clarity in the derived pulsatile parameter expressions, harmonics-dependence of the $\xi(t)$ waveform was not identified in Mirsky's study. The influence of axial initial tension on the $\xi(t)$ waveform was not considered.

The previous theoretical study conducted by the author [18] derived the mathematical expressions of various pulsatile parameters in terms of pulsatile pressure, but the influence of harmonics and wave reflection on the pulsatile parameters was not considered and the waveforms of different pulsatile parameters could not be plotted. Thus, how harmonics and wave reflection affects the waveforms of pulsatile parameters were not obtained. Meanwhile, the related numerical studies [19,20] on radial and axial displacement of the arterial wall examined pulsatile wave propagation in time domain, and thus were incapable of identifying the influence of harmonics and wave reflection of pulsatile parameters with mathematical clarity. Moreover, these numerical studies did not consider the two initial tensions and thus did not identify the effect of $\tau_{\theta 0}$ on wave velocity and the effect of τ_{x0} on the $\xi(t)$ waveform.

In this study, pulsatile wave propagation is analyzed in the frequency domain for mathematical relations between pulsatile parameters under different harmonics, which allows identifying the influence of harmonics on pulsatile parameters. The influence of wave reflection on the pulsatile parameters is determined by their directions. Afterward, the pulsatile parameters with harmonics and wave reflection are expressed in the time domain, and consequently, their waveforms can be calculated, based on the harmonic values of measured pulsatile pressure and blood flow rate. The influence of wave reflection and harmonics on the five pulsatile parameters is summarized in Table 8. This table clearly explains the difference in waveform between $\xi(t)$, $\tau_w(t)$, and $Q(t)$, and predicts the identical waveform for $\Delta p(t)$ and $\eta(t)$. Table 9

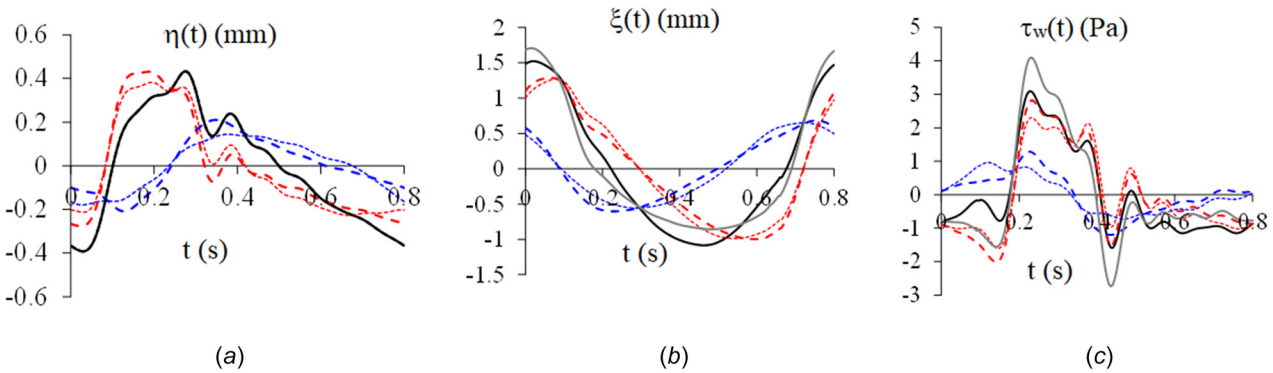

Fig. 4 Calculated waveforms of: (*a*) radial wall displacement $\eta(t)$ and (*b*) axial wall displacement $\xi(t)$ and (*c*) wall shear stress $\tau_w(t)$ at the AA under $\gamma = 1$, $\tau_{\theta 0} = 0.1$, and $\tau_{x0} = 0.2$ with the forward and backward waves (dotted lines for the forward and backward waves: based on Eq. (20), dashed lines for the forward and backward waves: based on Eq. (18); solid black line: sum of the forward and backward waves based on Eq. (20), solid gray line: sum of the forward and backward waves based on Eq. (18))

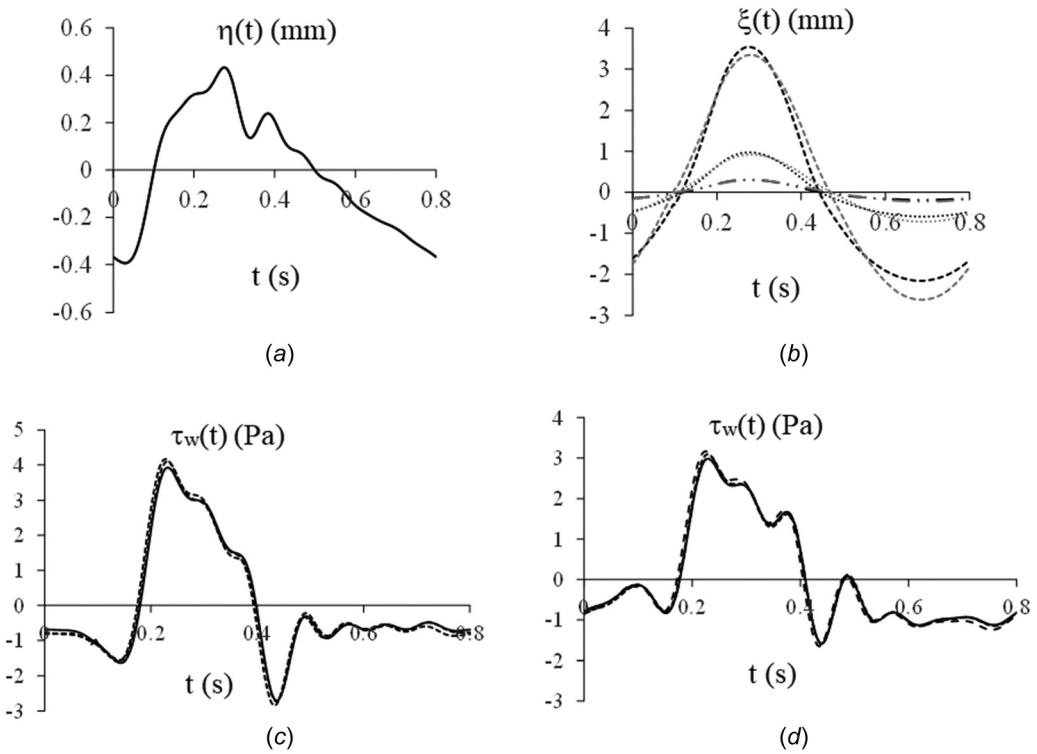

Fig. 5 Calculated waveforms at the AA under $\tau_{\theta 0} = \tau_{x0} = 0.1$: (*a*) radial wall displacement $\eta(t)$, (*b*) the axial wall displacement $\xi(t)$, (*c*) wall shear stress $\tau_w(t)$ based on Eq. (18), and (*d*) wall shear stress $\tau_w(t)$ based on Eq. (20) (black lines: based on Eq. (18), gray lines: based on Eq. (20); dash-dot line: $\gamma = 3$, dotted line: $\gamma = 1$, dashed line: $\gamma = 1/3$; solid black line: $\xi(t) = 0$)

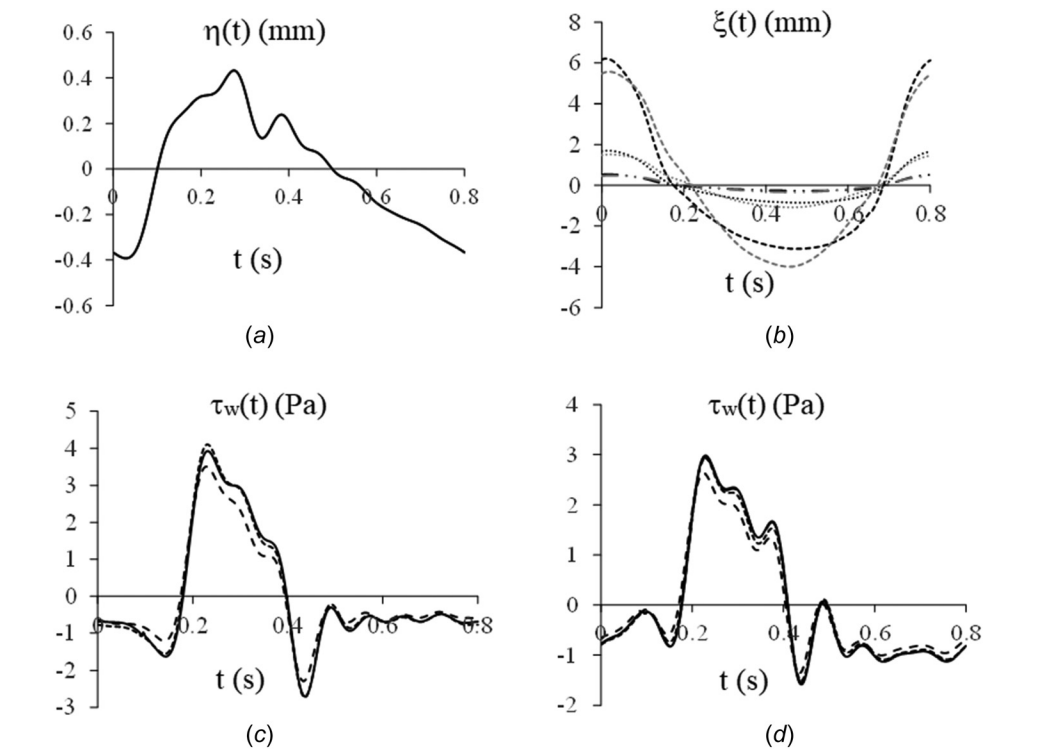

Fig. 6 Calculated waveforms at the AA under $\tau_{\theta 0} = 0.1$ and $\tau_{x0} = 0.2$: (*a*) radial wall displacement $\eta(t)$, (*b*) the axial wall displacement $\xi(t)$, (*c*) wall shear stress $\tau_w(t)$ based on Eq. (18), and (*d*) wall shear stress $\tau_w(t)$ based on Eq. (20) (black lines: based on Eq. (18), gray lines: based on Eq. (20); dash-dot line: $\gamma = 3$, dotted line: $\gamma = 1$, dashed line: $= 1/3$; solid black line: $\xi(t) = 0$)

Table 8 Influence of wave reflection and harmonics on the five pulsatile parameters measured in clinical studies

	Wave reflection	Harmonics-dependence
Δp	Augment	No
η	Augment	No
ξ	Reduce	Yes
Q	Reduce	No
τ_w	Reduce	Yes

summarizes the influence of harmonics on wave velocity and the related terms in Eq. (16). The harmonics-independence of $\eta(t)$ and $Q(t)$ arises from the harmonics-independence of $1+mF_{10}$. The value of τ_{x0} affects the dependence of $1+m$ on harmonics and thus alters the $\xi(t)$ waveform, as shown in Figs. 3(*b*) and 4(*b*). The influence of harmonics on mF_{10} remains the same under the two values of τ_{x0}, and thus the $\tau_w(t)$ waveform remains unchanged, as shown in Figs. 3(*c*) and 4(*c*). Different wave reflections only noticeably affect the maximum and minimum values of $\tau_w(t)$. Thus, characteristic impedance might not be a very effective indicator of arterial health.

As the input, $\Delta p(t)$ is expected to determine the harmonic values for all the rest pulsatile parameters at an artery. However, the measured $\Delta p(t)$ cannot separate its forward wave from its backward wave by itself, as shown in Eq. (16*a*). The harmonic values of the measured $\Delta p(t)$ are from the forward and backward waves of $\Delta p(t)$. To obtain the forward and backward waves of $\Delta p(t)$, the measured $Q(t)$ is needed, as shown in Eq. (17). As such, $\Delta p(t)$ and $Q(t)$ are both needed to determine the harmonic values at an artery. The waveforms of $\eta(t)$, $\xi(t)$, and $\tau_w(t)$ can then be calculated. Although it is well recognized that an arterial pulse signal is a collection of harmonics of the heart rate [13], there are no studies on what factors determine the harmonic values at an artery, to the author's best knowledge.

4.2 Physiological Implications. Due to its ease access, the carotid artery (CA) is focused on for $\xi(t)$ measurement [2–7]. The measured $\xi(t)$ waveform is found to be different from the $\tau_w(t)$ waveform at the CA, although $\tau_w(t)$ is commonly considered as the source for causing $\xi(t)$ [4,5]. As shown above, this difference can be explained by the different harmonics-dependence of $\tau_w(t)$ and $\xi(t)$ and the contribution of the $\partial\eta/\partial x$ term with a factor of $(T_{x0}-T_{\theta 0})$ to $\xi(t)$. Due to its difficult access, the AA is not measured for the $\xi(t)$ waveform yet, and thus no comparison can be made for the calculated $\xi(t)$ waveform.

Based on Eqs. (4*a*) and (4*b*), pulsatile pressure causes radial wall displacement, while wall shear stress and the $\partial\eta/\partial x$ term cause axial wall displacement. Given that pulsatile pressure (a few kPa) is three order of magnitude higher than wall shear stress (a few Pa), it is understandable that radial wall displacement is coupled into axial wall displacement, but axial wall displacement does not affect radial wall displacement and blood flow rate. This may validate that clinical studies can neglect axial wall displacement for these common clinical measures and their relations. Thus, in terms of facilitating blood flow in an artery, axial wall displacement is trivial, as compared with radial wall displacement.

Table 9 Dependence of the wave velocity and the related terms in Eq. (16) on harmonics under different axial initial tension

	$\tau_{\theta 0}=0.1$, $\tau_{x0}=0.1$	$\tau_{\theta 0}=0.1$, $\tau_{x0}=0.2$
c	No	No
$1+mF_{10}$	No	No
$1+m$	Yes	No
mF_{10}	Yes	Yes

According to Secs. 2 and 3, radial wall displacement reflects circumferential elasticity and circumferential initial tension, while axial wall displacement amplitude and waveform manifest axial elasticity and axial initial tension, respectively. This may explain the reason why axial wall displacement and radial wall displacement correlate with CV risk factors differently. Although axial wall displacement at the CA has been extensively measured in recent years, its physical mechanism is still unclear. One study found that other than wall shear stress, there should be other pulsatile forces in the axial direction [25]. This work identifies the $\partial\eta/\partial x$ term with a factor of $(T_{x0}\text{-}T_{\theta 0})$ as another pulsatile force causing axial wall displacement. Since axial wall displacement is more sensitive to subclinical atherosclerosis, it might suggest that axial elasticity and axial initial tension are also indicators of arterial health, and are affected by subclinical atherosclerosis to a larger extent, as compared with circumferential elasticity.

Although axial wall displacement is trivial in facilitating blood flow in an artery, its identified clinical values suggest its importance to arterial health. Moreover, axial wall displacement allows axial strain/strain to occur in the arterial wall. According to the tissue-level studies on vascular homeostasis [8,9], other than wall shear stress, circumferential stress and axial stress of the arterial wall is also important for maintaining vascular homeostasis. As analyzed here, clinical values and vascular homeostasis of axial wall displacement are derived from axial elasticity and aixal initial tension of the arterial wall, given that these two mechanical properties predominantly dictate axial wall displacement. Currently, axial elasticity and axial initial tension cannot be measured in vivo, due to a lack of the related theories [2–7,25]. The influence of axial elasticity on axial displacement amplitude and the influence of axial initial tension on axial displacement waveform may provide a theoretical basis for their measurement and study of vascular homeostasis in vivo.

4.3 Study Limitations. There are four major limitations to this study. First, there is no measured $\xi(t)$ waveform at the AA for comparison with the calculated one. The $\xi(t)$ waveform is commonly measured at the CA. Since the harmonic values of pulsatile pressure and blood flow rate at the CA are not available, no calculation of the $\xi(t)$ waveform at the CA can be conducted. Second, strictly speaking, the arterial wall at the AA is a thick-walled tube, given its ratio of h/a is 0.15. For examining the influence of harmonics and wave reflection on pulsatile parameters with mathematical clarity, a thin-walled tube is used to model the arterial wall. Third, the study neglects the curved and tapering geometrical nature of the arterial wall. Lastly, this study does not consider a possible contribution to $\xi(t)$ and $\tau_w(t)$ from the Lamb wave. Nevertheless, these limitations may affect the quantitative relations between pulsatile parameters and the arterial wall mechanical properties, but are not expected to alter the roles and physiological implications of axial wall displacement and two initial tensions in the Young wave revealed in this study.

5 Conclusion

In this paper, a theoretical study is presented on radial and axial displacement of the arterial wall for deriving wave velocity and pulsatile parameter expressions under the influence of harmonics and wave reflection. With the harmonic values of measured pulsatile pressure and blood flow rate at the AA in the literature, the waveforms of radial wall displacement, axial wall displacement, and wall shear stress are calculated with different values of orthotropicity and axial initial tension for the influence of axial elasticity and axial initial tension on these pulsatile parameters. While blood flow rate and radial wall displacement follow the harmonic distribution of pulsatile pressure, axial wall displacement and wall shear stress show different harmonics-dependence. The amplitude and waveform of axial wall displacement are predominantly dictated by axial elasticity and axial initial tension, respectively. Although axial wall displacement is trivial in terms of facilitating

blood flow in an artery, its clinical values for the detection of subclinical atherosclerosis and its role in vascular homeostasis suggest the importance of axial elasticity and axial initial tension to arterial health. The obtained results provide a theoretical basis for the measurement of axial elasticity and axial initial tension in vivo and the study of vascular homeostasis in vivo.

Funding Data

- National Science Foundation (NSF) Division of Chemical, Bioengineering, Environmental, and Transport Systems (Grant No. 1936005; Funder ID: 10.13039/100000146).

References

[1] Willemet, M., and Alastruey, J., 2015, "Arterial Pressure and Flow Wave Analysis Using Time-Domain 1-D Hemodynamics," Ann. Biomed. Eng,. **43**(1), pp. 190–206.

[2] Yli-Ollila, H., Laitinen, T., Weckström, M., and Laitinen, T. M., 2016, "New Indices of Arterial Stiffness Measured From Longitudinal Motion of Common Carotid Artery in Relation to Reference Methods, a Pilot Study," Clin. Physiol. Funct. Imag., **36**(5), pp. 376–388.

[3] Gepner, A. D., McClelland, R. L., Korcarz, C. E., Young, R., Kaufman, J. D., Mitchell, C. C., and Stein, J. H., 2019, "Carotid Artery Displacement and Cardiovascular Disease Risk in the Multi-Ethnic Study of Atherosclerosis," Vasc. Med., **24**(5), pp. 405–413.

[4] Au, J. S., Ditor, D. S., MacDonald, M. J., and Stöhr, E. J., 2016, "Carotid Artery Longitudinal Wall Motion is Associated With Local Blood Velocity and Left Ventricular Rotational, but Not Longitudinal, Mechanics," Physiol Rep., **4**(14), p. e12872.

[5] Au, J. S., Bochnak, P. A., Valentino, S. E., Cheng, J. L., Stöhr, E. J., and MacDonald, M. J., 2018, "Cardiac and Haemodynamic Influence on Carotid Artery Longitudinal Wall Motion," Exp. Physiol., **103**(1), pp. 141–152.

[6] Taivainen, S. H., Yli-Ollila, H., Juonala, M., Kähönen, M., Raitakari, O. T., Laitinen, T. M., and Laitinen, T. P., 2018, "Influence of Cardiovascular Risk Factors on Longitudinal Motion of the Common Carotid Artery Wall," Atherosclerosis, **272**, pp. 54–59.

[7] Taivainen, S. H., Yli-Ollila, H., Juonala, M., Kähönen, M., Raitakari, O. T., Laitinen, T. M., and Laitinen, T. P., 2017, "Interrelationships Between Indices of Longitudinal Movement of the Common Carotid Artery Wall and the Conventional Measures of Subclinical Arteriosclerosis," Clin. Physiol. Funct. Imag., **37**(3), pp. 305–313.

[8] Cardamone, L., Valentín, A., Eberth, J. F., and Humphrey, J. D., 2009, "Origin of Axial Prestretch and Residual Stress in Arteries," Biomech. Model Mechanobiol., **8**(6), pp. 431–446.

[9] Humphrey, J. D., Eberth, J. F., Dye, W. W., and Gleason, R. L., 2009, "Fundamental Role of Axial Stress in Compensatory Adaptations by Arteries," J. Biomech., **42**(1), pp. 1–8.

[10] Gao, M., Cheng, H. M., Sung, S. H., Chen, C. H., Olivier, N. B., and Mukkamala, R., 2017, "Estimation of Pulse Transit Time as a Function of Blood Pressure Using a Nonlinear Arterial Tube-Load Model," IEEE Trans. Biomed. Eng., **64**(7), pp. 1524–1534.

[11] Womersley, J. R., 1955, "XXIV. Oscillatory Motion of a Viscous Liquid in a Thin-Walled Elastic Tube—I: The Linear Approximation for Long Waves," Lond. Edinb. Dublin Philos. Mag. J. Sci., **46**(373), pp. 199–221.

[12] Atabek, H. B., 1968, "Wave Propagation Through a Viscous Fluid Contained in a Tethered, Initially Stresses, Orthotropic Elastic Tube," Biophys J., **8**(5), pp. 626–649.

[13] Mirsky, I., 1967, "Wave Propagation in a Viscous Fluid Contained in an Orthotropic Elastic Tube," Biophys J., **7**(2), pp. 165–186.

[14] Cox, R. H., 1969, "Comparison of Linearized Wave Propagation Models for Arterial Blood Flow Analysis," J. Biomech., **2**(3), pp. 251–65.

[15] Klip, W., Van Loon, P., and Klip, D. A., 1967, "Formulas for Phase Velocity and Damping of Longitudinal Waves in Thick-Walled Viscoelastic Tubes," J. Appl. Phys., **38**(9), pp. 3745–3755.

[16] Holzapfel, G. A., and Ogden, R. W., 2010, "Constitutive Modelling of Arteries," Proc. R. Soc. A., **466**(2118), pp. 1551–1597.

[17] Humphrey, J. D., 2009, "Vascular Mechanics, Mechanobiology, and Remodeling," J. Mech. Med. Biol., **09**(02), pp. 243–257.

[18] Smith, S. M., Marin, J., Adams, A., West, K., and Hao, Z., 2022, "Radial and Axial Motion of the Initially Tensioned Orthotropic Arterial Wall in Arterial Pulse Wave Propagation," ASME J. Med. Diag., **5**(2), p. 021004.

[19] Bukač, M., and Čanić, S., 2013, "Longitudinal Displacement in Viscoelastic Arteries: A Novel Fluid-Structure Interaction Computational Model, and Experimental Validation," Math. Biosci. Eng., **10**(2), pp. 295–318.

[20] Wang, Z., Wood, N. B., and Xu, X. Y., 2015, "A Viscoelastic Fluid-Structure Interaction Model for Carotid Arteries Under Pulsatile Flow," Int. J. Numer. Method Biomed., Eng., **31**(5), p. e02709.

[21] Carew, T. E., Vaishnav, R. N., and Patel, D. J., 1968, "Compressibility of the Arterial Wall," Circ. Res., **23**(1), pp. 61–8.

[22] Anliker, M., Moritz, W. E., and Ogden, E., 1968, "Transmission Characteristics of Axial Waves in Blood Vessels," J. Biomech., **1**(4), pp. 235–246.

[23] Lucas, C. L., Wilcox, B. R., Ha, B., and Henry, G. W., 1988, "Comparison of Time Domain Algorithms for Estimating Aortic Characteristic Impedance in Humans," IEEE Trans. Biomed. Eng., **35**(1), pp. 62–68.

[24] Jagielska, K., Trzupek, D., Lepers, M., Pelc, A., and Zieliński, P., 2007, "Effect of Surrounding Tissue on Propagation of Axisymmetric Waves in Arteries," Phys. Rev. E Stat. Nonlin. Soft Matter Phys., **76**(6 Pt 2), p. 066304.

[25] Ahlgren, Å. R., Steen, S., Segstedt, S., Erlöv, T., Lindström, K., Sjöberg, T., Persson, H. W., Ricci, S., Tortoli, P., and Cinthio, M., 2015, "Profound Increase in Longitudinal Displacements of the Porcine Carotid Artery Wall Can Take Place Independently of Wall Shear Stress: A Continuation Report," Ultrasound Med. Biol., **41**(5), pp. 1342–1353.